Journal of Catalysis 286 (2012) 153–164

Contents lists available at SciVerse ScienceDirect

Journal of Catalysis

journal homepage: www.elsevier.com/locate/jcat

Deoxygenation mechanisms on Ni-promoted MoS_2 bulk catalysts: A combined experimental and theoretical study

M. Ruinart de Brimont [a], C. Dupont [a], A. Daudin [a,*], C. Geantet [b], P. Raybaud [a]

[a] IFP Energies nouvelles, Rond point de l'échangeur de Solaize, BP3, 69360 Solaize, France
[b] IRCELYON, UMR 5256 CNRS – Université Lyon1, 2 avenue Albert Einstein, 69626 Villeurbanne cedex, France

ARTICLE INFO

Article history:
Received 5 July 2011
Revised 12 October 2011
Accepted 23 October 2011
Available online 12 December 2011

Keywords:
Hydrodeoxygenation
Decarbonylation
Ester
Aldehyde
NiMoS
MoS_2
Ni_3S_2
Mechanism
Density functional theory

ABSTRACT

Through a combined experimental and density functional study, we investigate the deoxygenation of ethyl heptanoate catalyzed by three relevant unsupported (bulk) transition metal sulfide catalysts: MoS_2, Ni_3S_2 and Ni-promoted MoS_2 (with various Ni/Mo ratio). Two pathways compete for this reaction: hydrodeoxygenation (HDO) and decarboxylation/decarbonylation (DCO). It is shown experimentally that the presence of Ni either in the NiMoS mixed phase or in the Ni monosulfide phase may change the selectivity between the HDO and DCO pathway. To understand the origin of this selectivity, we study the deoxygenation pathways of two relevant intermediates: carboxylic acid and aldehyde. In particular, DFT calculations highlight that the aldehyde decarbonylation occurs via its dehydrogenation into the alkanoyl and/or ketene intermediates on the Ni_3S_2 (111) surface. These pathways are found to be more favorable on Ni_3S_2 than on MoS_2-based catalysts. This trend is explained by the presence of Ni_3 triangular facets on Ni_3S_2 (111) enhancing the formation of the unsaturated alkanoyl and/or ketene intermediates as well as the CO product. We finally propose a detailed analysis of the promoting effect of Ni on MoS_2, when present in the NiMoS structure.

1. Introduction

Due to global warming and air pollution, the Kyoto protocol in 1997 prompts the European Union (EU) to make a commitment to reduce the emissions of greenhouse gases by 5.2% over 2008–2012 period (with respect to the levels observed in 1990). In addition, the necessity of a stronger energetic independence of petroleum resources encourages the EU to impose on the petroleum industry to incorporate biofuels with an energetic yield of 10% in 2020 (Directive 2009/30/CE L140/88).

Biodiesel is usually obtained by transesterification of vegetable oils (like fatty acid methyl ester) and is blended with diesel fuel. An interesting alternative to produce renewable diesel is the hydrotreatment (including hydrodeoxygenation) of vegetable oils leading to fully deoxygenated paraffinic diesel with excellent combustion properties. Many works have reported the feasibility of this type of process since more than 30 years [1–5]. Transition metal sulfide catalysts such as MoS_2 phase promoted by Co (CoMoS) or Ni (NiMoS) supported on γ-Al_2O_3 are known to be active for the deoxygenation reaction [5], and numerous experimental works have investigated the reactivity of aliphatic compounds (esters, carboxylic acids, real vegetable oils) over supported transition metal sulfide (TMS) catalysts [6–16]. It is well accepted that the conversion of vegetable oils (or triglycerides) follows a reaction scheme involving two deoxygenation routes [14]. The first one is the hydrodeoxygenation pathway (labeled as HDO in what follows) preserving the number of carbon atoms of the ester aliphatic chain and leading to water formation. The second one is made of the decarboxylation/decarbonylation pathways (labeled as DCO) leading to hydrocarbons with one carbon atom removed from the original alkyl chain and to carbon oxides (CO, CO_2). Şenol et al. have studied the deoxygenation of methyl heptanoate, *n*-heptanoic acid and 1-heptanol over sulfided NiMoS and CoMoS/γ-Al_2O_3 catalysts [9]. They proposed a reaction scheme for the conversion of methyl heptanoate involving heptanoic acid as a primary product followed by the formation of heptanal. Without direct evidence, they suggest that heptanal could be the oxygenated intermediate leading selectively to the HDO or DCO pathway. However, the decarbonylation mechanism of heptanal (if there is) remains to be investigated. These authors have also shown that the HDO route will conduct to alkanes and alkenes through the deoxygenation of alcohol obtained from heptanal.

According to recent experimental works on the deoxygenation of rapeseed oils, Kubička and Kaluža showed that the nature of the supported TMS phase modifies the selectivity of the deoxygenation pathways [14]. On the one hand, the NiS_x active phase

* Corresponding author. Fax: +33 437702066.
E-mail address: antoine.daudin@ifpen.fr (A. Daudin).

0021-9517/$ - see front matter © 2011 Elsevier Inc. All rights reserved.
doi:10.1016/j.jcat.2011.10.022

supported on γ-Al_2O_3 yields only products resulting from the DCO pathway. On the other hand, MoS_2 supported on γ-Al_2O_3 yields mostly hydrocarbons produced by the HDO pathway. In the presence of the Ni-promoted MoS_2 phase supported on Al_2O_3, hydrocarbons are produced from the two reaction pathways. Kubička and Kaluža [14] also studied the effect of Ni/(Ni + Mo) atomic ratio in the range 0.2–0.4 and concluded that this atomic ratio does not play any significant role neither on the activity nor on the selectivity.

However, although these experimental observations are rather interesting, no rational interpretation based on the molecular scale's study of the mechanisms has been proposed to explain the sensitivity of the reaction pathways with respect to the TMS phases. In addition, deoxygenation reactions are known to be highly sensitive to the support effects. For example, in the case of guaiacol conversion, Bui et al. pointed out that the use of various supports for CoMoS catalyst induces the formation of heavy compound (involving acido-basic properties of the support) and influences directly the conversion and deoxygenation of guaïacol [17,18]. More precisely, oxygenated compounds such as 2-ethylphenol in presence of γ-alumina under HDT conditions lead to disproportionation products and isomerization products as demonstrated recently by Romero et al. [19]. Hence, if we want to avoid any unwished effects induced by the support, it is of interest to investigate the catalytic behaviors of relevant unsupported TMS. To our knowledge, such a fundamental study has never been undertaken.

Thanks to significant advances in density functional theory (DFT) calculations applied to the atomic scale's description of the Co(Ni)MoS active phases [20–22], it became possible to investigate the hydrodeoxygenation mechanism of aldehyde on the M-edge of NiMoS and MoS_2 phases [23]. In particular, the promoting role of Ni on the MoS_2 phases was highlighted for both the C═O hydrogenation and the C—OH bond breaking steps. It was explained by the key role of the Ni—Mo mixed site catalyzing the nucleophilic substitution mechanism between the alcohol and the Mo—SH group. However, further experimental and theoretical investigations are still needed for a better understanding of the rather complex deoxygenation mechanisms and particularly the decarbonylation route.

By combining well-defined experiments and density functional theory (DFT) calculations, the present work proposes a kinetic and molecular scale's study of the deoxygenation mechanisms of relevant oxygenated molecules (ester, carboxylic acid and aldehyde) so as to provide rational guides to identify the optimal catalytic systems for the hydrotreating of renewable feedstocks. We firstly investigate the deoxygenation reaction of ethyl heptanoate over three relevant unsupported transition metal sulfide catalytic phases: MoS_2, Ni_3S_2 and Ni-promoted MoS_2 (with different Ni/Mo atomic ratios). Bulk TMS active phases are synthesized, characterized and tested in order to avoid any support effects and to determine the intrinsic properties of these TMS phases. Ethyl heptanoate is used as model molecule for triglycerides contained in vegetable oils. Indeed, this molecule is representative of the ester function and of the alkyl chain of triglycerides. Then, for an improved understanding of the reaction mechanism, we focus on the deoxygenation reaction of heptanoic acid and heptanal over the same sulfide catalysts using the same reaction conditions. The effect of Ni/Mo molar ratios is carefully studied on both reactants. DFT calculations are simultaneously used to investigate the HDO and DCO pathways at a molecular level on the NiMoS and Ni_3S_2 (1 1 1) surface to identify the hydrodeoxygenation and decarbonylation pathways. Finally, combining both the experimental data and the DFT results, we propose new insights to explain the origin of the HDO and DCO pathways.

2. Experimental and theoretical methods

2.1. Catalysts preparation

Molybdenum disulfide was prepared by the thermal decomposition of ammonium thiomolybdate [24,25]. First of all, the ammonium tetrathiomolybdate precursor $(NH_4)_2MoS_4$ (ATM) was synthesized from ammonium heptamolybdate (8 g in 40 cc of distilled water) and ammonium sulfide in water solution (40–48 wt%) at 333 K during one hour (for the list of chemicals see Table S1 in supplementary information). Then, the red solution freshly obtained was placed in iced water during three hours to form ATM red crystals. These crystals are then washed with isopropanol and dried under nitrogen flow at room temperature. Finally, molybdenum disulfide was obtained after sulfidation at 673 K (heating rate of 3.3 K/min) during four hours under H_2/H_2S (15 mol%) flow (1.8 $L.h^{-1}.g^{-1}$).

Ni-promoted MoS_2 catalysts (NiMoS) were prepared from ATM [26]. Nickel nitrate was diluted in acetone, and then the solution was dropped on ATM. Acetone was removed by stirring at room temperature. A black solid was obtained and sulfided at 673 K (heating rate of 3.3 K/min) during four hours under H_2/H_2S (15 mol%) flow (1.8 L/h/g). NiMoS catalysts were synthesized with Ni/Mo molar ratios (x) equal to 0.1, 0.2 and 0.43 and labeled as NiMoS(x).

Ni_3S_2 catalytic phase was prepared by a low temperature method [27] from an aqueous solution containing sodium disulfide (Na_2S) added dropwise to an aqueous solution of nickel nitrate. Molar ratio S/metal was equal to 1.2. The mixture was stirred during two hours at room temperature. Then, the black powder precipitate was washed with distilled water, dried under nitrogen and sulfided at 573 K (heating rate of 3.3 K/min) during four hours under a H_2/H_2S (15 mol%) flow. A second thermal treatment under hydrogen with the same temperature and time conditions was necessary to obtain the Ni_3S_2 phase.

2.2. Characterization methods

Fresh sulfided phases were characterized before catalytic tests by X-ray photoelectron spectroscopy (XPS), X-ray diffraction (XRD) using the Panalytical X'Pert Pro instrument, transmission electron microscopy (TEM) using the FEI Tecnai FEG instrument, and elemental analysis (using the FLASH 2000-CHNS technique) to identify the exact nature of the catalytic phases. After catalytic tests, the catalysts were also characterized by XRD and elemental analysis (X-ray fluorescence, XRF and combustion CHNS) to verify that no significant structural modification has occurred. The specific surface areas (using the Micromeritics ASAP 2420 instrument) were also evaluated before and after catalytic tests.

The XPS experiments were carried out with a ESCA KRATOS Axis Ultra spectrometer equipped with a Al monochromator source ($h\upsilon$ = 1486.6 eV). The surface of analysis was 700 $*$ 300 μm. The excitation power was 15 kV $*$ 10 mA and the fixed pass energy was 40 eV. The samples were prepared under argon to avoid the formation of sulfate. Binding energies (BE) of the various elements have been referenced to the C1s level of the contamination carbon at 284.6 eV [28]. The elemental surface composition of the catalytic phases and the atomic ratio of sulfur/metal (S/Me) were determined from the intensity of the metal and sulfur peaks (with a relative uncertainty of 20%). Moreover, a quantitative XPS analysis of the different phases in presence (mixed sulfides, monosulfides, or oxides) was done according to the methodology detailed in previous works [29–31].

2.3. Reaction conditions

Ethyl heptanoate was first used as a model molecule to explore the conversion of triglycerides contained in vegetable oils. Before

each test, to ensure a complete sulfidation of the active phase, the catalyst was resulfided *in situ* in H_2/H_2S (15 mol%) flow during four hours at 673 K (heating rate was 3.3 K/min) at atmospheric pressure. Then, the catalytic test was carried out in a fixed-bed reactor in gas phase at 523 K under a total pressure of 1.5 MPa. The molar ratio H_2/feed was 350 Nl/l, which corresponds to a hydrogen partial pressure of 1.44 MPa in the reactor (see Table S2 in supplementary information). The model feed was composed of 6 wt% (3.4×10^{-3} MPa) of ethyl heptanoate in 5×10^{-2} MPa of dodecane. In addition, we investigated the conversion of heptanal (and heptanoic acid), using similar reaction conditions: $T = 523$ K, with a total pressure of 1.5 MPa and a partial pressure of heptanal of 4.8×10^{-3} MPa (6 wt%). Dimethyldisulfide (10^{-4} MPa) was also added to maintain the sulfidation state of the catalyst (corresponding to 500 ppm wt S in the liquid feed). The product distribution for several conversion rates was obtained by varying the contact time (see Table S3 in supplementary information). The catalytic activity was measured after stabilization of the catalyst (the time on stream for each contact time is around 15 h). In our conditions, no significant deactivation of the various catalysts was noticed.

2.4. Chromatographic analysis and activity measurements

The reaction products were analyzed online in gas phase using an Agilent 6890 chromatograph equipped with a PONA capillary column (length 50 m, i.d. 0.2 mm, film thickness 0.5 μm) and a flame ionization detector. Temperature starts from 308 K to 453 K (5 K/min) with a stage of thirty minutes at final temperature. Products' identification was performed by GC–MS coupling (GC–MS Quad). In order to quantify the products, the external calibration of the chromatograph was carried out with well-quantified solutions of each reactant and products.

The conversion, the deoxygenation products yield and the selectivity of each product were determined by the following Eqs. (1)–(3). All conversions were measured after catalyst stabilization (the time on stream for each contact time is around 15 h, and no significant deactivation of the various catalysts was noticed).

$$\textit{Conversion yield}\ (\%) = \frac{\sum m_i}{\sum m_i + m_r} \times 100 \tag{1}$$

$$\textit{Deoxygenation products yield}\ (\%) = \frac{\sum m_{dj}}{\sum m_i + m_r} \times 100 \tag{2}$$

$$\textit{Selectivity}_{\textit{producti}}\ (\%) = \frac{m_i}{\sum m_i} \times 100 \tag{3}$$

where m_i is the molar percentage of the product i, m_r is the molar percentage of the reactant (ethyl heptanoate or heptanal) and m_{dj} is the molar percentage of the deoxygenated product j.

Reaction rates were calculated assuming a first-order reaction with plug-flow reactor model. Specific deoxygenation rates, called r_s (mol g^{-1} h^{-1}), were calculated for the monometallic phases (MoS_2, Ni_3S_2) using the following equation:

$$r_s = \frac{F}{m} \ln\left(\frac{100}{100 - X}\right) \tag{4}$$

where X is the molar percentage of deoxygenated product (mol%) measured for similar conversion level (close to 20 mol%), F is the molar flow of products (mol/h) and m is the mass of catalyst (g).

2.5. Theoretical methods

Periodic density functional theory calculations were performed using the VASP code [32,33]. General gradient approximation with PW91 [34,35] for the exchange correlation functional and the projector augmented wave (PAW) [36] are used. The cutoff energy for the plane-wave basis was fixed to 500 eV, and the Brillouin zone integration was performed on a $(3 \times 3 \times 1)$ Monkhorst–Pack k-point mesh. The geometry optimization was completed when forces became smaller to the threshold of 0.03 eV $Å^{-1}$.

Periodic supercells of the NiMoS system were modeled according to our previous study [37] by considering the chemical potential of sulfur in the gas phase as used in experiments ($T = 523$ K and $p(H_2S)/p(H_2) \sim 0.01$). In brief, four molybdenum sub-surface layers covered by one mixed Ni—Mo metallic row were considered, with a 50% promotion rate and a 12.5% sulfur coverage (Fig. 1a and b). Hence, each supercell contains one sulfur atom and four metallic (2 Ni plus 2 Mo) atoms, which corresponds to the thermodynamic equilibrium as defined in [37]. All further technical details about the model used are reported in [37]. Concerning the nickel monosulfide model, we consider the (1 1 1) surface of Ni_3S_2 which as been shown to be the predominant one under sulfo-reductive environment [38]. Moreover, according to the relatively low chemical potential of sulfur imposed by the experimental conditions, we assumed the presence of one S-vacancy on the (1 1 1) surface which thus exposes Ni_3 triangular facets surrounded by sulfur atoms. A five-layer slab with the Ni_3S_2 stoichiometry was considered, as represented in Fig. 1c and d. The two lowest planes were frozen in a bulk-like geometry, while the three uppermost layers are allowed to relax. The following parameters, $x = y = 11.52$ and $z = 25.64$ Å, were used for the supercell, represented in Fig. 1c and d.

For adsorption, only the lowest coverage, corresponding to one oxygenated molecule coadsorbed with one hydrogen molecule (for the hydrogenation steps), was studied. Besides, for sake of calculations size, derivatives of propanoate have been considered, instead of heptanoate as performed experimentally. Nevertheless, although it may slightly influence the absolute values, it will not modify the relative trends found for the hydrogenation and dehydrogenation steps of the —CH_2—CH=O group as a function of the active phase.

3. Results and discussion

3.1. Characterization

The physico-chemical properties of the unsupported catalysts before and after reaction determined by XRD, XPS, XRF and specific surface area are reported in Table 1. Characterizations by XRD and XPS before reaction show that expected phases were obtained. For nickel sulfide, a mixture of Ni_3S_2 and NiS (<5%) was observed. The minor presence of NiO detected by XPS (but not by XRD) indicates a slight contamination of the surface of NiMoS (0.2), NiMoS (0.43) and Ni_3S_2 catalysts due to re-oxidation. To prevent its formation, catalysts were re-sulfided *in situ* before each catalytic test (see Section 2.1). S/metal (Ni or Mo) molar ratios were obtained by bulk elemental analysis (from XRF and CHNS) and XPS. These ratios are consistent with the crystallographic data obtained by XRD. NiMoS catalysts are composed of three different catalytic phases: NiMoS, MoS_2 and nickel monometallic phases. Table 2 shows the weight composition of the NiMoS catalysts (derived from XPS analysis). The amount of NiMoS phase is relatively high in each mixed phase but depends on Ni/Mo atomic ratio (comprised between 42 at.% and 76 at.%). At the same time, the part of the nickel monometallic phase increases with the Ni/Mo molar ratio.

MoS_2 has the highest specific surface area (54 m^2/g), whereas nickel sulfide exhibits the lowest one (5 m^2/g). Adding nickel to MoS_2 phase implies a decrease in the specific surface area of NiMoS mixed catalyst with respect to pure MoS_2. We also point out that the specific surface area varies for each NiMoS catalyst: it

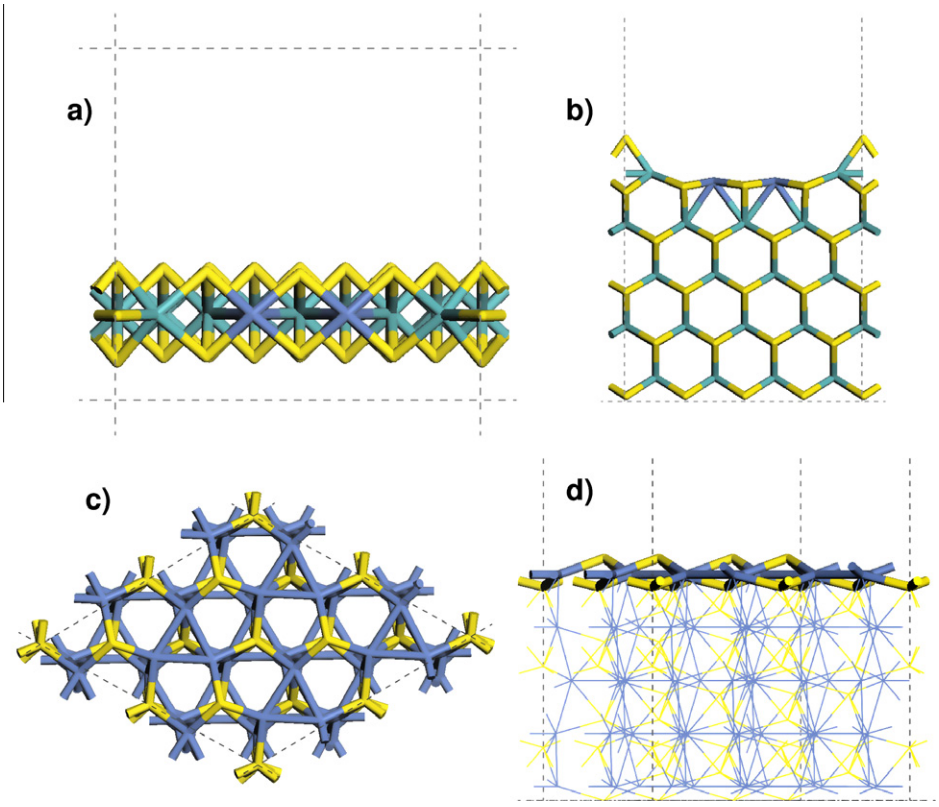

Fig. 1. Slab models used for the DFT simulation: (a) top view, (b) side view of the M-edge of the NiMoS phase; (c) top view, and (d) side view of the Ni_3S_2 (1 1 1) surface. Color legend: blue sticks: nickel, green sticks: molybdenum, yellow sticks: sulfur. (For interpretation of the references to color in this figure legend, the reader is referred to the Web version of this article.)

Table 1
Physico-chemical properties of the unsupported sulfide catalysts before and after the transformation of ethyl heptanoate.

Phases	Before reaction Identified phases by XRD	Attributed phases by XPS	S/Me atom (Me = Mo or Ni) by XPS	S/Me atom (Me = Mo or Ni) by XRF	Specific surface area (m^2/g)	After reaction Identified phases by XRD	C (wt%)	Specific surface area (m^2/g)
MoS_2	MoS_2	MoS_2	2.0	1.6	54	MoS_2	2.2	11
NiMoS (0.1)	MoS_2	NiMoS, NiS, MoS_2	2.1	2.2	13	MoS_2	6.3	9
NiMoS (0.20)	MoS_2	NiMoS, NiS, NiO, MoS_2	2.1	1.9	7	MoS_2	7.1	3
NiMoS (0.43)	MoS_2, NiS	NiMoS, NiS, NiO, MoS_2	2.0	2.4	29	MoS_2, Ni_3S_2	4.3	13
Ni_3S_2	Ni_3S_2, NiS	Ni_3S_2, NiS, NiO, NiOS	0.6	0.6	5	Ni_3S_2	1.1	2

Table 2
Evolution of the content of nickel engaged in mixed phase and in monometallic sulfide phase over NiMoS catalysts (atomic% obtained from XPS characterization).

NiMoS catalysts	$Ni_{(NiMoS)}$ (atomic%)	$Ni_{(NiSx)}$ (atomic%)
NiMoS (0.1)	1.3	0.4
NiMoS (0.2)	3.1	1.4
NiMoS (0.43)	3.3	4.6

fluctuates between 7 m^2/g and 29 m^2/g depending on the Ni/Mo ratio. This textural evolution between MoS_2 and NiMoS catalysts is attributed to the presence of segregated Ni monosulfide as detected by XPS.

All catalysts were also characterized after deoxygenation of ethyl heptanoate by XRD and elemental analysis (Table 1) to demonstrate the stability of catalytic phases. Indeed, no structural modification is noted except the partial reduction of NiS into Ni_3S_2 phase. The carbon content is relatively low (1.1–2.2 wt%) for monometallic catalyst, whereas NiMoS bimetallic phases had a higher carbon content (4.3–7.1 wt%). Specific surface area after reaction is lower than before test. The most important decrease is observed for the specific surface area of MoS_2 (11 m^2/g after reaction).

3.2. Reactivity of ethyl heptanoate

The conversion of ethyl heptanoate leads to the formation of deoxygenated and oxygenated compounds. The product distributions at various conversion rates were obtained by varying the contact time for the different catalysts. The results are reported in Figs. 2, 3 and 4. The variation of conversion as a function of contact time is also reported for the three catalysts in Fig. S5 in supplementary information (see also Section 3.4). At low conversion, ethyl heptanoate is systematically converted into oxygenated products: heptanoic acid, heptanol, heptanal and heptyl heptanoate. Heptanoic acid is the predominant oxygenated compound at low conversion for all catalysts which reveals the

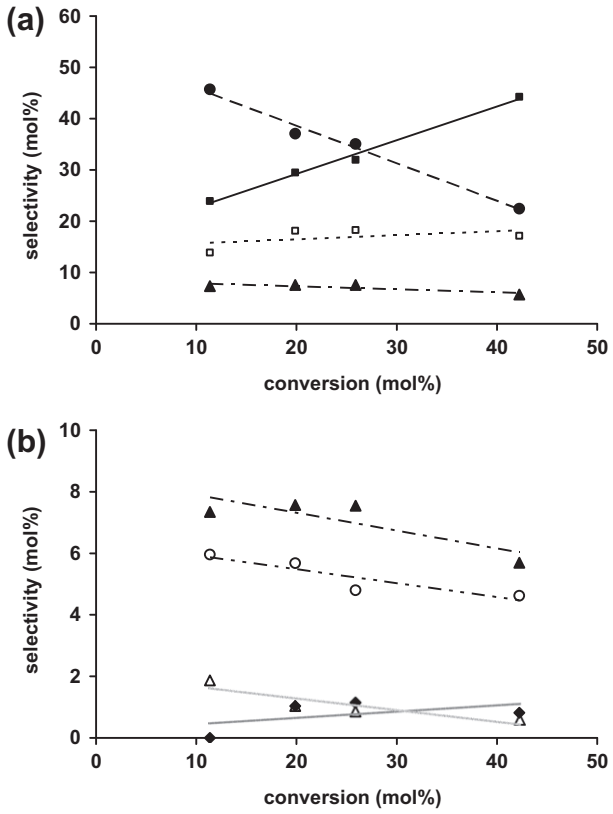

Fig. 2. Variation of the product selectivity (mol%) of the ethyl heptanoate deoxygenation as a function of conversion (mol%) on the MoS_2 phase: (a) main products, (b) minor products. (T = 523 K, P = 1.5 MPa, H_2/feed = 350 Nl/l). Legend: (●) heptanoic acid, (■) heptane, (□) heptenes; (▲) heptanol, (△) heptanal, (○) heptyl heptanoate, (♦) hexane.

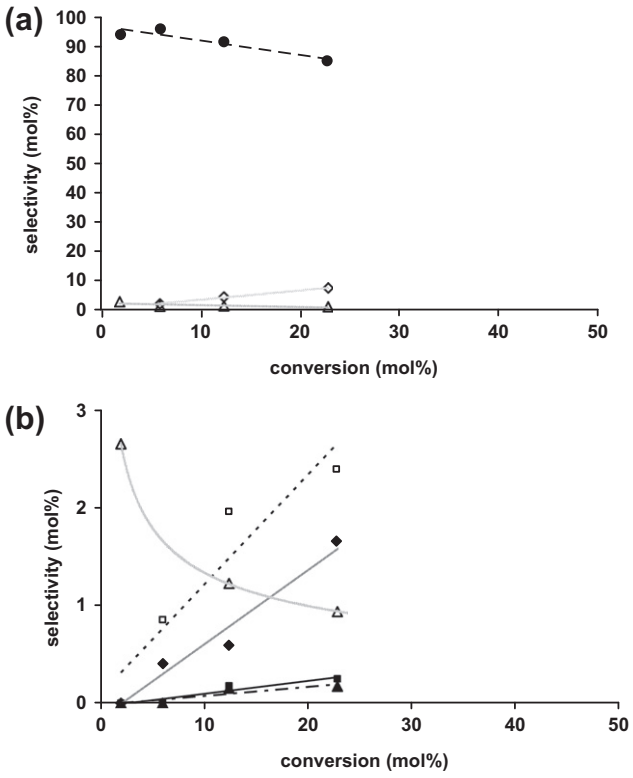

Fig. 3. Variation of the product selectivity (mol%) of the ethyl heptanoate deoxygenation as a function of conversion (mol%) on the Ni_3S_2 phase: (a) main products, (b) minor products. (T = 523 K, P = 1.5 MPa, H_2/feed = 350 Nl/l). Legend: (●) heptanoic acid, (■) heptane, (□) heptenes, (▲) heptanol, (△) heptanal, (○) heptyl heptanoate, (♦) hexane, (◇) hexenes.

refractory character of this oxygenated compound over all TMS and particularly over Ni monosulfide. Heptanal is detected over all catalysts even if it is not quantifiable on mixed phases. Heptyl heptanoate is observed in a non-negligible amount on most MoS_2-based catalyst but is not quantifiable on Ni_3S_2. The formation of this product points out the possible acido-basic character of MoS_2-based catalysts.

At higher conversion, these products are deoxygenated and lead to hydrocarbons as final products. The deoxygenated products are composed of aliphatic hydrocarbons, mainly alkenes (heptenes $C_7^=$ and hexenes $C_6^=$) and alkanes (heptane C_7 and hexane C_6). The formation of the C_7 and C_6-hydrocarbons suggests that two deoxygenation routes are taking place. The HDO pathway leads to C_7-hydrocarbons with the simultaneous release of water. The decarbonylation/decarboxylation pathways leading to C_6-hydrocarbons with the simultaneous formation of carbon oxides (CO and CO_2 not analyzed in the present work).

Table 3 summarizes the product distribution at a conversion around 20% for MoS_2, NiMoS and Ni_3S_2 catalysts. Oxygenated compounds are the most important products family over all the catalysts. The quantity of oxygenated compounds is close to 88 mol% over Ni_3S_2 catalyst but only 39.4 mol% over NiMoS (0.43). At this conversion, heptanoic acid appears again as the main product over all the catalytic phases, whereas heptanal is the minor one. Heptane is the main deoxygenated product over MoS_2, NiMoS (0.1) and NiMoS (0.2), while hexane and hexenes are the most important deoxygenated products over NiMoS (0.43) and Ni_3S_2, respectively. The alkenes/(alkanes + alkenes) ratio is the highest one for the Ni_3S_2 phase meaning that this phase is less hydrogenating than the other phases studied. On the contrary, the most hydrogenating phase is NiMoS (0.43) with an alkenes/(alkanes + alkenes) ratio equals to 0.25. These observations are coherent with previous results on alkene hydrogenation over TMS catalysts in similar reaction conditions [39]. The various products obtained are consistent with the previous works by Şenol et al. [9,10] over supported sulfide catalysts. According to these works, carboxylic acid was identified as a primary product on CoMoS/γ-Al_2O_3.

As a complementary analysis, we investigated the product distribution for the heptanoic acid deoxygenation reaction on NiMoS (0.43), Ni_3S_2 and MoS_2 catalysts. As reported in Table S4, we observe that on the three catalysts, the product distribution and HDO/DCO selectivity follow the same trend as for the ester deoxygenation reactions (Table 3). Moreover, starting from heptanoic acid as a reactant, we clearly observe the formation of aldehyde. We thus confirm that carboxylic acid is a primary product, for the conversion of ester, leading to the aldehyde intermediate on the unsupported TMS phases, as proposed by Şenol et al. for CoMoS/γ-Al_2O_3 [9,10].

3.3. Effect of the TMS phase on the HDO/DCO selectivity

For the NiMoS catalysts, the two main routes for the deoxygenation reaction, i.e. HDO and DCO, have been observed in previous studies on supported TMS catalysts [9,14]. We thus confirm this result on bulk TMS. It becomes now interesting to propose a more quantitative analysis of the role of Ni promoter on the HDO/DCO selectivity since the Ni-promoted MoS_2 phase contains not only the wished NiMoS mixed phase but also the Ni monometallic sulfided phase, as indicated by the XPS analysis (Table 2). From our catalytic data, the HDO/DCO selectivity is followed by the relative C_7 and C_6-hydrocarbon yields. Table 3 reports the $(C_6 + C_6^=)$/

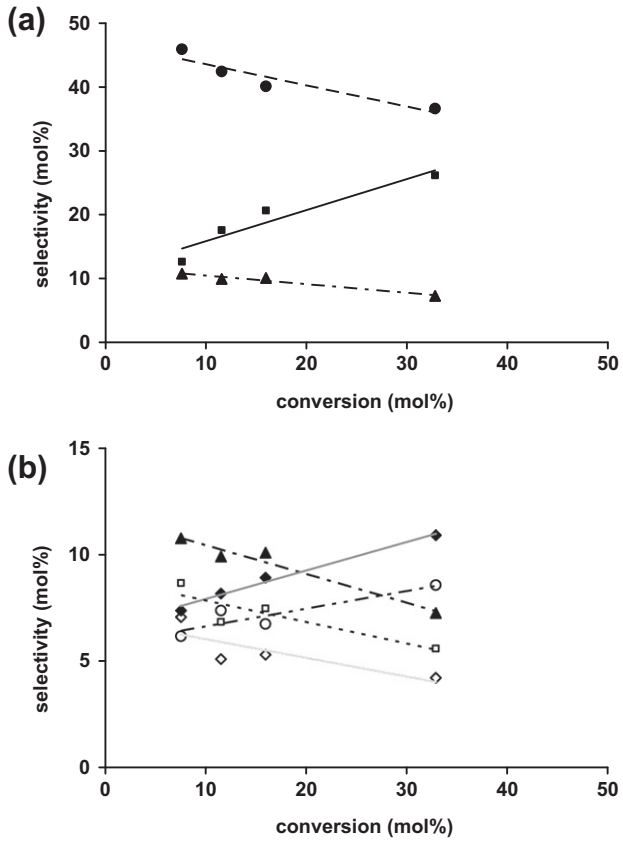

Fig. 4. Variation of the product selectivity (mol%) of the ethyl heptanoate deoxygenation as a function of conversion (mol%) on the unsupported NiMoS phase (Ni/Mo molar ratio = 0.2): (a) main products, (b) minor products. (T = 523 K, P = 1.5 MPa, H_2/feed = 350 Nl/l). Legend: (●) heptanoic acid, (■) heptane, (□) heptenes, (▲) heptanol, (○) heptyl heptanoate, (♦) hexane, (◇) hexenes.

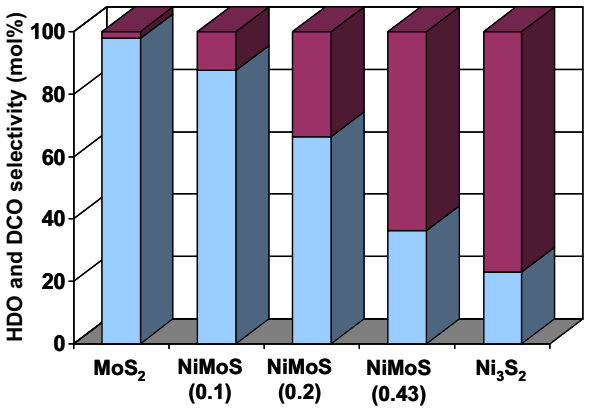

Fig. 5. HDO and DCO selectivity (expressed in mol% at a conversion close to 20 mol%) as a function of the TMS phases: MoS_2, Ni_3S_2 and NiMoS for various Ni/Mo molar ratios. Color legend: blue: HDO (mol%), purple: DCO (mol%). (For interpretation of the references to color in this figure legend, the reader is referred to the Web version of this article.)

$(C_7 + C_7^=)$ molar ratio as a function of the sulfide phases for similar conversions. On MoS_2, the deoxygenation of ethyl heptanoate leads mostly to C_7-hydrocarbons. Thus, the HDO pathway is predominant on the non-promoted MoS_2 phase as observed by Kubička and Kaluža [14] and Daudin and Chapus [40] in the case of γ-Al_2O_3-supported MoS_2. By contrast, on the nickel monosulfide catalyst, C_6-hydrocarbons are the most abundant among the deoxygenated products, which reveals that the DCO pathway is predominant on this phase.

On the NiMoS mixed phases, a non-negligible amount of C_6-hydrocarbons is observed even though it is significantly lower than on nickel monosulfide. Both HDO and DCO pathways take place during the deoxygenation of ethyl heptanoate. In addition, as illustrated in Table 3, the $(C_6 + C_6^=)/(C_7 + C_7^=)$ molar ratio increases as the Ni content increases. This evolution of the product selectivity for the HDO and DCO pathways on MoS_2, Ni_3S_2 and NiMoS as a function of the Ni/Mo ratio is clearly highlighted in Fig. 5. Without more accurate analysis, we suspect that the presence of Ni either in the monosulfide phase or in the NiMoS phase affects the pathways for the ester deoxygenation reaction. In what follows, we attempt to identify the origin of this trend.

3.4. Heptanal hydrodeoxygenation mechanisms

As previously mentioned, the results on the deoxygenation reaction of heptanoic acid reveal similar trends as for the ester conversion. In particular, the presence of heptanal is clearly observed during the acid deoxygenation (Table S4) and is considered as a critical reaction intermediate. Hence, for a better understanding of the deoxygenation mechanisms, we now focus on the reactivity of heptanal on the same unsupported catalytic phases: MoS_2, Ni_3S_2 and the NiMoS series. Fig. 6 represents the variation of the products selectivity as a function of heptanal conversion. Fig. S6 in supplementary information also reports the evolution of heptanal conversion as a function of contact time. The conversion of heptanal leads to formation of oxygenated and deoxygenated compounds. On the MoS_2-based catalysts, heptanol is the

Table 3
Conversion and product distribution of the ethyl heptanoate reaction (T = 523 K, P = 1.5 MPa, H_2/feed = 350 Nl/l).

Phases		MoS_2	NiMoS (0.1)	NiMoS (0.2)	NiMoS (0.43)	Ni_3S_2
Conversion (mol%)		19.9	20.9	16.0	21.7	22.8
Products families selectivity (mol%)	HDO	47.6	38.7	28.3	21.9	2.7
	DCO	1.0	5.4	14.3	38.7	9.1
	Intermediary oxygenated products	51.4	55.9	57.3	39.4	88.2
Products selectivity (mol%)	Hexane	1.0	1.6	8.9	27.9	1.7
	Hexenes	Traces	3.8	5.3	9.4	7.3
	Heptane	29.5	19.9	20.6	15.9	0.2
	Heptenes	18.1	19.0	7.5	5.2	2.4
	Heptanol	7.6	15.5	10.1	2.3	0.2
	Heptanal	1.0	1.2	Traces	Traces	0.9
	Heptanoic acid	37.0	27.9	40.1	33.4	85.1
	Heptyl heptanoate	5.7	11.6	6.8	2.2	Traces
Alkenes/(alkanes + alkenes)		0.37	0.51	0.30	0.25	0.84
$(C_6 + C_6^=)/(C_7 + C_7^=)$		0.02	0.14	0.51	1.77	3.38

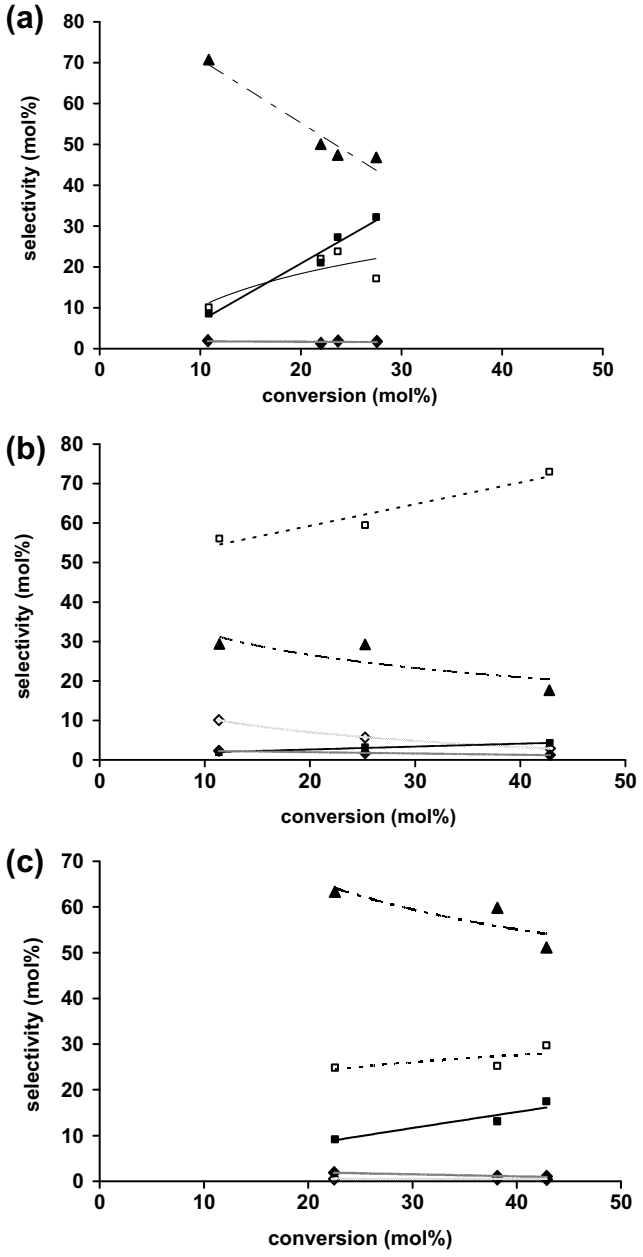

Fig. 6. Variation of the product selectivity (mol%) of heptanal deoxygenation as a function of conversion (mol%) on (a) MoS_2, (b) Ni_3S_2, c) NiMoS (Ni/Mo molar ratio = 0.2). (T = 523 K, P = 1.5 MPa, H_2/feed = 350 Nl/l). Legend: (■) heptane, (□) heptenes, (▲) heptanol, (♦) hexane, (◇) hexenes.

predominant product while heptenes are predominant on Ni_3S_2. Table 4 shows the product distribution obtained at a conversion close to 20 mol%. HDO products (heptane and heptenes) are thus the most predominant products on all the catalysts excepted on NiMoS (0.2) mixed phase. On NiMoS (0.2), oxygenated products are the most prevailing compounds (63.4 mol%). On MoS_2, $C_7^=$ and C_7 are predominant (nearly 97%) among the deoxygenated products as for the ethyl heptanoate conversion. On NiMoS catalysts, HDO products are even more predominant than for the ethyl heptanoate deoxygenation (Tables 3 and 4). This means that the heptanal hydrogenation is not rate determining and is significantly more favored than the decarbonylation pathways when heptanal is the starting reactant (in the absence of any other reactants or oxygenate intermediates). This observation is fully consistent with recent DFT calculations showing that either on MoS_2 or on NiMoS, the activation barriers for the aldehyde hydrogenation are smaller than the C—O bond breaking, which is the rate-limiting step for the heptanal deoxygenation reaction [23]. This explains why heptanal is first rapidly hydrogenated into heptanol, observed as the predominant product. More surprisingly, although DCO products are observed on Ni_3S_2, HDO products are predominant on Ni_3S_2 catalyst (table 4), whereas they were minor products of ethyl heptanoate deoxygenation on Ni_3S_2. As for the MoS_2 and NiMoS catalysts, this trend is explained by the rapid intrinsic hydrogenation of aldehyde on Ni_3S_2 catalyst when starting from the aldehyde molecule as a unique reactant.

In order to compare more closely the hydrogenation steps of aldehyde into alcohol for the NiMoS and Ni_3S_2 phases, we have calculated the reaction and activation energies for the two monohydrogenation steps of propanal into propanol by DFT. For that purpose, we have considered relevant active sites located on the Ni-promoted M-edge of NiMoS in a similar way as in [23] Simultaneously, we consider the active sites located on the Ni_3S_2 (1 1 1) surface as represented in Fig. 1c and d. The values reported in Fig. 7 show that on the Ni_3S_2 (1 1 1) surface, the thermodynamic balance remains exothermic for the two hydrogen transfers from two surface Ni—SH groups to the aldehyde molecule. On NiMoS, the reaction pathway involves both Ni—H and Mo—SH groups and the thermodynamic balance is significantly more exothermic than on Ni_3S_2. Besides, activation energy barriers for C—H and O—H formation are very low on NiMoS ($\approx$17 kJ mol^{-1}) [23], while the lowest value evaluated for Ni_3S_2 is 30 kJ mol^{-1} for O—H formation, and C—H formation presents activation energy barriers higher than 50 kJ mol^{-1}. This comparative thermodynamic and kinetic analysis explains the experimental observations revealing that the HDO activity is lower on Ni_3S_2 than on NiMoS, although it remains possible on Ni_3S_2.

Table 4
Conversion and product distribution of the heptanal deoxygenation at a conversion close to 20 mol% (T = 523 K, P = 1.5 MPa, H_2/feed = 350 Nl/l).

Phases		MoS_2	NiMoS (0.1)	NiMoS (0.2)	NiMoS (0.43)	Ni_3S_2
Conversion (mol%)		21.9	19.6	22.6	34.8	25.2
Products families selectivity (mol%)	HDO	59.6	53.2	34.0	51.0	62.9
	DCO	1.8	1.7	2.6	3.7	7.8
	Intermediary oxygenated products	38.6	45.0	63.4	45.3	29.3
Products selectivity (mol%)	Hexane	1.7	1.7	1.9	2.6	1.9
	Hexenes	Traces	Traces	0.7	1.1	5.8
	Heptane	39.5	22.9	9.2	18.7	3.3
	Heptenes	17.5	30.2	24.9	32.3	59.5
	Heptanol	36.9	44.9	63.3	45.3	29.3
Alkenes/(alkanes + alkenes)		0.30	0.55	0.70	0.61	0.93
$(C_6 + C_6^=)/(C_7 + C_7^=)$		0.03	0.03	0.08	0.07	0.12

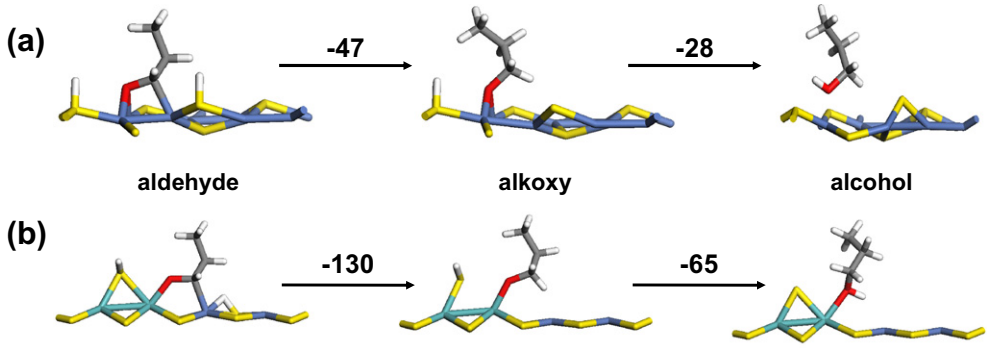

Fig. 7. The two subsequent monohydrogenation steps of aldehyde leading to alcohol (via alkoxy intermediate) and the corresponding DFT reaction energies (in kJ mol^{-1}) on (a) the Ni_3S_2 (1 1 1) surface and (b) the M-edge of NiMoS. As for reference [23], the simulated molecules are C_3 oxygenates.

3.5. Analysis of the promoting effect of Ni

Focusing first on the activation of the C=O bond as a function of Ni content, we investigate whether a promoting effect of nickel may exist for such reactions. First, we studied the reactivity of heptanal as a model molecule. The quantitative determination of the weight distribution of the different sulfided phases synthesized in the NiMoS series (Table 2) enables the evaluation of the intrinsic activities of the mixed phases normalized either by gram or by exposed surface area (evaluated after reaction) as reported in Fig. 8 (and Table S7 in Supplementary information). The comparison of the deoxygenation and HDO rates for the heptanal conversion shows that NiMoS mixed catalysts are the most active, with increasing rates for increasing Ni/Mo molar ratios. In addition, NiMoS (0.43) exhibits deoxygenation and HDO activities increased by a factor of 5–10 with respect to the MoS_2 and Ni_3S_2 monosulfides. These results highlight the promoting effect of Ni on the MoS_2 phase for the heptanal reaction. This can be also interpreted as a manifestation of the "synergy effect" induced by the formation of the NiMoS phase, as observed in hydrodesulfurization and hydrogenation reactions [41–43]. This promoting effect is also explained by considering our recent DFT calculations [23], where it was shown that the Ni promoter present at the edge of the MoS_2 crystallite induces a lowering of the activation energies with respect to non-promoted MoS_2 for both the C=O hydrogenation and C—OH bond breaking steps. Moreover, the DFT calculations undertaken on the Ni_3S_2 (1 1 1) surface for the present work and discussed in the previous paragraph show that the heptanal hydrogenation is thermodynamically and kinetically less favored on Ni_3S_2 than on NiMoS which also justifies the higher activity measured on NiMoS.

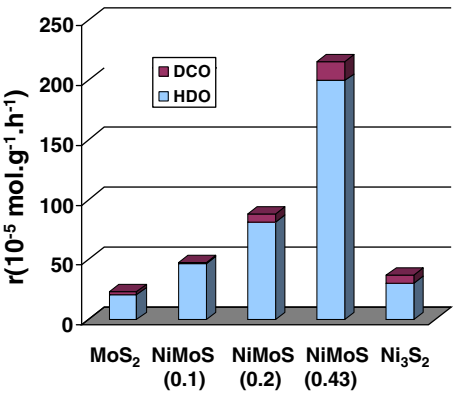

Fig. 8. Decarbonylation (DCO) and hydrodeoxygenation (HDO) rates (in mol g^{-1} h^{-1}) for the heptanal deoxygenation reaction (normalized per gram of catalyst) as a function of the catalysts.

This analysis unambiguously elucidates the promoting effect of Ni on the MoS_2 phase for the heptanal deoxygenation, when present in the NiMoS structure.

Regarding the ester deoxygenation reaction, the interpretation of the observed trend is more complex due to the competition between the DCO and HDO pathways on NiMoS catalysts, on the one hand, and due to the presence of large amounts of the carboxylic acid by-products, on the other hand. For the low or medium level of conversion investigated here, the promoting effect of Ni is thus not straightforward. Considering first the HDO pathway, MoS_2 also exhibits the highest specific HDO rate of all catalysts, as reported in Table 5. Hence, the measured catalytic rates seem to highlight the absence of promoting effect of Ni for the ethyl heptanoate HDO. This trend significantly differs from the one observed for the heptanal HDO and may result from the presence of other by-products such as carboxylic acid which affects the intrinsic HDO of ethyl heptanoate. Since the HDO reaction rates are evaluated in the present work at low or medium conversion, heptanoic acid remains the most important product (Figs. 2–4).

This result can also be analyzed by considering the overall reaction rate as reported in Table 6. Heptanal is about 3–3.5 times more active than ester on the NiMoS and Ni_3S_2 catalyst. By contrast,

Table 5
Specific deoxygenation, HDO and DCO rates for the various unsupported catalysts for ethyl heptanoate conversion.

Catalyst	*r* (deoxygenation) (10^{-5} mol g^{-1} h^{-1})	*r* (HDO) (10^{-5} mol g^{-1} h^{-1})	*r* (DCO) (10^{-5} mol g^{-1} h^{-1})
MoS_2	37.9	37.0	0.9
NiMoS (0.1)	18.1	15.8	2.3
NiMoS (0.20)	18.8	12.3	6.5
NiMoS (0.43)	75.3	26	49.3
Ni_3S_2	2.0	0.5	1.5

Table 6
Consumption rate of heptanoic acid, ethyl heptanoate and heptanal over NiMoS (0.43), Ni_3S_2 and MoS_2 (T = 523 K, P = 1.5 MPa, H_2/feed = 350 Nl/l, 6 wt% of oxygenate compound).

Catalysts	Feed	Specific activity (10^{-5} mol g^{-1} h^{-1})	Relative specific activity
NiMoS (0.43)	Heptanoic acid	47	1
	Ethyl heptanoate	124	2.6
	Heptanal	436	9.3
Ni_3S_2	Heptanoic acid	5	1
	Ethyl heptanoate	18	3.6
	Heptanal	57	11.4
MoS_2	Heptanoic acid	32	1
	Ethyl heptanoate	77	2.4
	Heptanal	180	5.6

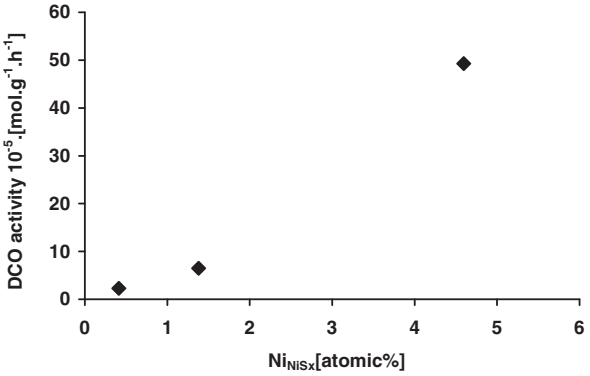

Fig. 9. Decarbonylation/decarboxylation (DCO) rates for the ester deoxygenation reaction (normalized per gram of catalyst) as a function of Ni_{NiSx} content (determined by XPS analysis).

heptanoic acid is about 3 times less active than ester. This implies that the carboxylic acid deoxygenation, and more precisely its hydrogenolysis into heptanal, is the rate-determining step and affects the promoting effect of Ni. Moreover, according to previous DFT calculations [23], carboxylic acid exhibits competitive adsorption energies on the edge site of NiMoS, which may be at the origin of inhibiting effects perturbing the promoting effect in this range of conversion. For instance, the large amount of acid accumulated on the catalyst surface may significantly perturb the supply of hydrogen required for achieving the subsequent HDO step of heptanal. Hence, the hydrogenolysis of heptanoic acid may induce an overconsumption of hydrogen in its local surface environment. As a consequence, the lack of hydrogen required for heptanal HDO may favor a dehydrogenation pathway instead. This point is further discussed in the next section.

If we now consider the DCO rates also reported in Table 5, it appears that the DCO activity depends on the Ni content of the catalyst. The atomic percentage of the monometallic Ni sulfide phase (mainly Ni_3S_2 in reaction conditions) detected by XPS on the Ni-promoted systems increases from 0.4 on the NiMoS (0.1) phase, up to 4.6 in NiMoS (0.43) (Table 2). As illustrated in Fig. 9, the quantity of residual monometallic nickel sulfide present in the Ni-promoted MoS_2 phases seems to be correlated with the increase in their DCO rates. In particular, the deoxygenation rate of NiMoS (0.43) is the highest one with a major contribution of DCO (Table 5). The Ni_3S_2 phase presents the lowest specific deoxygenation rate, with a predominant DCO contribution. As a consequence, we suspect that the strong increase observed for the DCO rate on this NiMoS catalyst with a high Ni/Mo ratio may result from the presence of the residual Ni monosulfide phase and their morphologic modification in the presence of MoS_2 active phase. To corroborate this, we undertook complementary TEM analyses showing that the dispersion of NiS_x crystallite is high. Indeed, the Ni monosulfide phase particles were not detected by TEM, whereas the particle sizes are ranging from 70 to 100 nm for the reference Ni monosulfide bulk phase. This dispersion effect on the Ni monosulfide phase is consistent with the significant increase in the DCO rate observed on NiMoS (0.43).

3.6. Proposed reaction mechanisms for aldehyde decarbonylation

To elucidate whether the DCO pathway originates from the presence of Ni in the monosulfide phase, we further investigate the reaction pathways of heptanal deoxygenation by DFT calculations. We now explore whether a dehydrogenation pathway of heptanal is possible as a precursor for its decarbonylation. As previously suggested, this scenario would be favored by a lack of hydrogen at the catalytic and by the presence of competitive adsorbates such as the carboxylic acid which consumes hydrogen for its hydrogenolysis and/or may block the hydrogen diffusion to heptanal. In that case, dehydrogenation steps of heptanal may occur and initiate the DCO pathway. The calculated pathways and their energy variations are represented for NiMoS and for Ni_3S_2 on Figs. 10 and 11, respectively.

We suggest that it may first involve an alkanoyl intermediate leading to carbon monoxide and C_{n-1} alkane by C—C hydrogenolysis. Fig. 10 shows that the first dehydrogenation step of aldehyde which involves the transfer of one H atom from the carbon atom of carbonyl group is not thermodynamically favorable (+83 KJ.mol^{-1}) on NiMoS. Besides, the competition between this endothermic process and propanal hydrogenation (Fig. 7) that highly favored both thermodynamically and kinetically prevents dehydrogenation mechanism on NiMoS. Thus, this result clearly confirms that the reverse hydrogenation step is predominant on NiMoS. By contrast, on the Ni_3S_2 (1 1 1) surface, it appears that the first dehydrogenation step is slightly exothermic (−6 KJ.mol^{-1}), which is also less favored than the reverse hydrogenation step. However, the reaction energy difference between the monohydrogenation step and the dehydrogenation one is significantly less pronounced on Ni_3S_2 (+41 KJ.mol^{-1}) than on NiMoS (+213 KJ.mol^{-1}). Considering two possible subsequent steps, the alkanoyl intermediate may first lead to alkane by direct C—C hydrogenolysis involving surface H transfer. The reaction energy is slightly more exothermic for Ni_3S_2 (−86 KJ.mol^{-1}) than for NiMoS (−62 KJ.mol^{-1}). Hence, while NiMoS presents the first endothermic dehydrogenation step, on Ni3S2, this

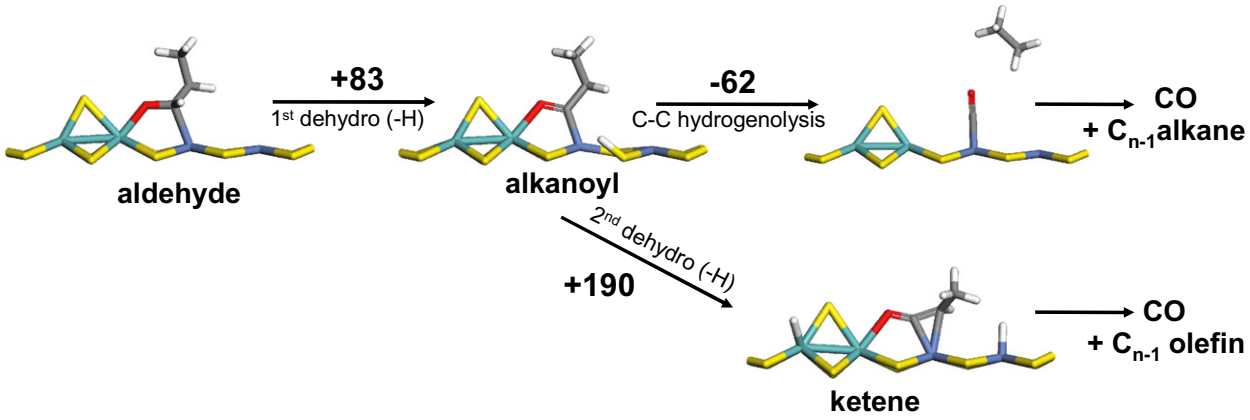

Fig. 10. Dehydrogenation and decarbonylation steps proposed for the aldehyde (propanal) conversion into CO and alkane or alkene (via the ketene intermediate) on NiMoS. The reaction energies are expressed in kJ mol^{-1}. As for reference [20], the simulated molecules are C3 oxygenates.

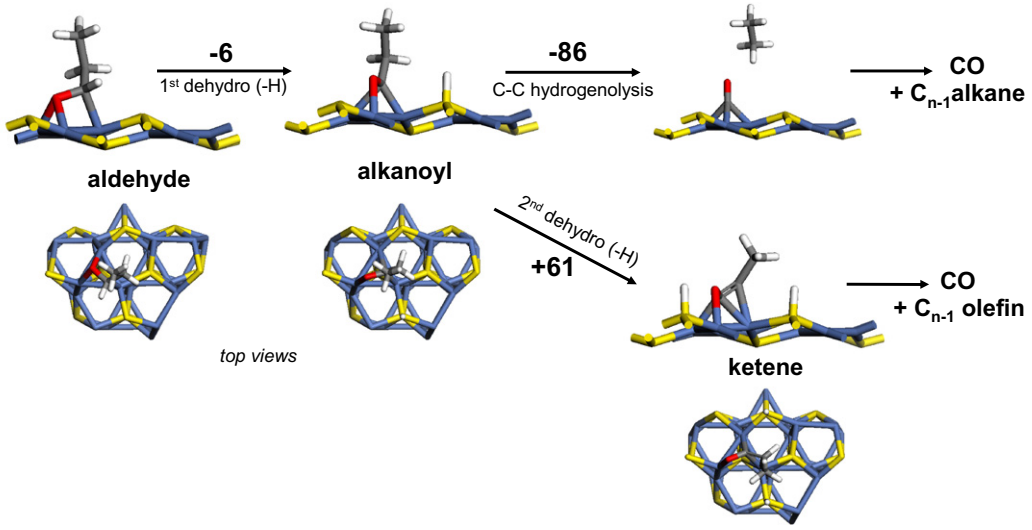

Fig. 11. Dehydrogenation and decarbonylation steps proposed for the aldehyde (propanal) conversion into CO and alkane or alkene on the Ni_3S_2 (1 1 1) surface. The reactions energies are expressed in kJ mol^{-1}.

step can directly compete with the reverse hydrogenation. These two results show that DCO initiated by the heptanal dehydrogenation is thermodynamically favored on Ni_3S_2 (111).

A second pathway involving a subsequent dehydrogenation step from the alkanoyl to the ketene intermediate can also be mentioned. It appears to be significantly less endothermic on Ni_3S_2 (+61 KJ.mol^{-1}) than on NiMoS (+190 KJ.mol^{-1}). If we assume the Hammond postulate, we expect that activation energies for these steps would follow a similar trend. Moreover, these energy differences calculated for the two systems are large enough to allow us to conclude that DCO is definitively preferred on Ni_3S_2.

These results are explained by the local structure and electronic properties of the Ni_3S_2 (1 1 1) surface, which exhibits Ni_3 triangular facets where the 3-fold hollow sites are favorable for the stabilization of the unsaturated alkanoyl and ketene intermediates as it occurs on purely metallic surface (see also top views in Fig. 11). By contrast, the two neighboring Ni—Mo edge sites are more constrained and do not allow a sufficient stabilization of these unsaturated intermediates. To a certain extent, this trend is also valid for the CO molecule which is also strongly stabilized in the 3-fold hollow configuration on the Ni_3S_2 (1 1 1) surface. The metallic character of the bulk Ni_3S_2 was already highlighted in a previous DFT investigation of the electronic properties of TMS [44] where a density of states analysis reveals a predominant occupation of Ni 3d states at the Fermi level. Interestingly, it is well known that purely metallic catalyst favors decarbonylation/decarboxylation route [45,46]. We suspect that this metallic character of Ni_3S_2 catalyst is at the origin of the DCO pathway.

From the experimental point of view, slightly higher value of the $(C_6 + C_6^=)/(C_7 + C_7^=)$ ratio is observed for Ni_3S_2 than for NiMoS and MoS_2 (Table 4). This is also consistent with the previous DFT analysis of the thermodynamic balance of the dehydrogenation and hydrogenation pathways, showing that dehydrogenation is potentially more favorable on Ni_3S_2. In the case of the ethyl heptanoate conversion, the formation of (C_6 and $C_6^=$) products is significantly increased, as illustrated by the $(C_6 + C_6^=)/(C_7 + C_7^=)$ ratios in Table 3. This is particularly true for Ni_3S_2 where a large amount of carboxylic acid is observed. At the same time, the amount of heptanol is significantly lower than on MoS_2 or NiMoS (0.1). This means that the hydrogenation pathway of heptanal is hindered. The presence of large amount of carboxylic acid at the catalytic surface may induce a depletion of hydrogen molecules and thus favor the aldehyde dehydrogenation particularly on the Ni_3S_2 phase, where the thermodynamic balance is less endothermic.

3.7. Summary on the reaction pathways

In summary, we propose two main mechanisms of the deoxygenation of ethyl heptanoate by hydrodeoxygenation (Fig. 12a) and by decarbonylation (Fig. 12b) or decarboxylation (Fig. 12c).

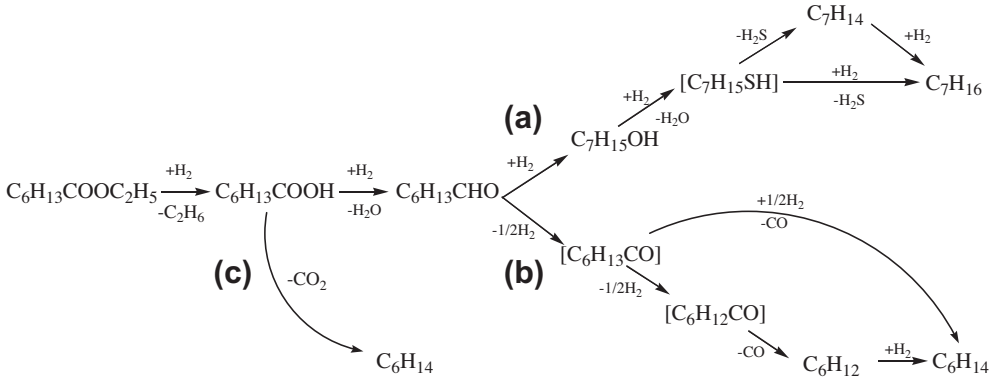

Fig. 12. Proposed mechanisms of the ethyl heptanoate conversion (excluding hydrolysis and esterification reactions) (a) by hydrodeoxygenation (HDO) occurring preferentially on MoS_2-based catalysts, (b) by decarbonylation, (c) decarboxylation (DCO) occurring on Ni_3S_2 catalyst.

Heptanoic acid is formed by the hydrogenolysis of ester on the sulfided active phase. Heptanal is then formed by hydrogenolysis of carboxylic acid (the predominant observed intermediate). For the HDO pathway, heptanal is easily hydrogenated into heptanol if sufficient hydrogen atoms are available at the catalytic surface. The recent DFT study on this HDO pathway on NiMoS and MoS_2 phases showed that alcohol is first transformed into thiol [23] through a nucleophilic substitution mechanism, and then heptane is obtained by hydrodesulfurization of thiol. Thiol can also be transformed into heptenes by an elimination mechanism [47]. Another possibility would be that heptenes may be formed by the direct dehydration of heptanol and then hydrogenated to form C_7, although this pathway is less probable on pure sulfide phase (not represented). In presence of an oxide support, this cannot be excluded. This HDO pathway is thus predominant on MoS_2 and NiMoS catalysts as observed experimentally.

For the DCO routes (Fig. 12b and c), two possible pathways may be invoked at this stage of our investigation. Even if we cannot exclude that heptanoic acid may be directly transformed into hexane by direct decarboxylation (Fig. 12c), our present study based also on DFT investigation proposes that heptanoic acid is transformed via the heptanal intermediate into hexane or hexenes by a sequence of dehydrogenation/decarbonylation steps of heptanal. Mind that heptanal is observed in significant amount during the heptanoic acid deoxygenation. According to this mechanism, heptanal would be first transformed into the heptanoyl intermediate (highly reactive and not observed experimentally) by a first monodehydrogenation step. Then, two possible pathways may occur: the first one is the direct C—C hydrogenolysis leading to alkane, and the second one is a subsequent dehydrogenation into a ketene intermediate leading to alkene, which is observed in a rather large amount on Ni monosulfide. This decarbonylation pathway is preferentially observed on Ni_3S_2 phase due to the local surface structure with Ni_3 triangular facets similar to metallic surfaces. On Ni-promoted MoS_2 phases, it is attributed to the presence of a residual Ni_3S_2 phase. In addition, and according to DFT calculations, this decarbonylation pathway is intrinsically less favorable than the hydrogenation one and is not predominant when starting from heptanal alone. It is thus suspected to be enhanced by the presence of inhibiting species such as carboxylic acid which prevents the access of hydrogen to heptanal.

4. Conclusion

Three relevant unsupported sulfide phases, MoS_2, Ni_3S_2 and Ni-promoted MoS_2, were evaluated for catalyzing the deoxygenation of ethyl heptanoate, in a fixed-bed reactor and in gas phase, as a model reaction for hydrotreatment of vegetable oils. In the absence of catalytic support, we first found that the nature of the TMS catalytic phase affects the deoxygenation pathways. On the MoS_2 bulk phase, the reaction is highly selective for the HDO pathway and leads to the formation of C_7-hydrocarbons, whereas on the Ni_3S_2 phase, the reaction follows preferentially the DCO pathway and the predominant deoxygenated products are C_6-hydrocarbons. On Ni-promoted MoS_2 phases, both reaction pathways were found to be competitive and the Ni/Mo ratio impacts the HDO/DCO selectivity. Since the Ni_3S_2 phase is simultaneously detected by XPS on those mixed phases, we propose that the DCO pathway originates from the presence of this residual Ni_3S_2 phases.

For a better understanding of the whole mechanism. The reactivity of the heptanal intermediate was also studied by experiments and DFT calculations. The results show that the reaction of deoxygenation follows preferentially the HDO pathway over all the catalysts. Thus, the HDO heptanal is clearly preferred than the decarbonylation/decarboxylation pathways when heptanal is used as the sole reactant. In addition, a clear promoting effect of Ni on the MoS_2 phase was found for the heptanal hydrodeoxygenation. This result is consistent with recent DFT calculations showing that the energy barriers for C═O hydrogenation and C—OH bond breaking are smaller on NiMoS with respect to MoS_2. This can be considered as a manifestation of the synergy effect as already known in hydrodesulfurization. By contrast, no clear promoting effect of Ni was observed for the HDO reaction of ethyl heptanoate which was explained by the detrimental role of carboxylic acid on the HDO pathway. Simultaneously, the high amount of carboxylic acid enhances the decarbonylation pathway on heptanal. This effect was specifically observed on the Ni monosulfide phase and on the Ni-promoted MoS_2 phase with a high Ni/Mo ratio. According to DFT calculations, the dehydrogenation pathway of aldehyde into alkanoyl and/or ketene intermediates is more thermodynamically favored on Ni_3S_2 than on MoS_2-based phases. This is attributed to the metallic character of Ni_3 triangular facets on the Ni_3S_2 (1 1 1) surface.

Hence, this work highlights the dual role of the nickel promoter added to MoS_2 phases. On the one hand, Ni present in the NiMoS mixed phase acts as a true promoter of hydrodeoxygenation reaction involving the aldehyde intermediate. On the other hand, Ni present in Ni monosulfide enhances the decarbonylation pathway. The control of the amount of residual nickel sulfide phases in the Ni-promoted system is a key parameter for tuning the HDO/DCO selectivity in vegetable oils deoxygenation. We hope that this work will help for a rational understanding of the impact of transition metal sulfides and more particularly Ni sulfide species on the deoxygenation pathways.

Acknowledgments

M. Ruinart de Brimont thanks IFP Energies nouvelles and ANRT for PhD grant. The authors thank also Christèle Legens, Philippe Lecour and Isabelle Clemençon for XPS and DRX analysis and fruitful discussions.

Appendix A. Supplementary material

Supplementary data associated with this article can be found, in the online version, at doi:10.1016/j.jcat.2011.10.022.

References

[1] P. Nunes, D. Brodzki, G. Bugli, G. Djega-Mariadassou, Rev. Inst. Fr. Pétr. 41 (3) (1986) 421.
[2] M. Stumborg, A. Wong, E. Hogan, Bioresour. Technol. 56 (1996) 13.
[3] W.K. Craig, D.W. Douglas, US Patent, 4992,605, 1991.
[4] T. Kalnes, T. Marker, D.R. Shonnard, Int. J. React. Eng. 5 (2007) 1.
[5] O. Weisser, S. Landa, Sulphide Catalysts, Their Properties and Applications, Pergamon Press, 1973.
[6] G.N. da Rocha Filho, D. Brodzki, G. Djéga-Mariadassou, Fuel 72 (1993) 543.
[7] E.-M. Ryymin, M.L. Honkela, T.-R. Viljava, A.O.I. Krause, Appl. Catal. A Gen. 358 (2009) 42.
[8] O.I. Senol, T.-R. Viljava, A.O.I. Krause, Catal. Today 106 (2005) 186.
[9] O.İ. Şenol, E.-M. Ryymin, T.-R. Viljava, A.O.I. Krause, J. Mol. Catal. A: Chem. 268 (2007) 1.
[10] O.İ. Şenol, T.-R. Viljava, A.O.I. Krause, Catal. Today 100 (2005) 331.
[11] O.İ. Şenol, T.-R. Viljava, A.O.I. Krause, Appl. Catal. A: Gen. 326 (2007) 236.
[12] O.İ. Şenol, E.-M. Ryymin, T.-R. Viljava, A.O.I. Krause, J. Mol. Catal. A: Chem. 277 (2007) 107.
[13] P. Šimáček, D. Kubička, G. Šebor, M. Pospíšil, Fuel 88 (2009) 456.
[14] D. Kubička, L. Kaluža, Appl. Catal. A: Gen. 372 (2010) 199.
[15] G.W. Huber, P. O'Connor, A. Corma, Appl. Catal. A: Gen. 329 (2007) 120.
[16] B. Donnis, R.G. Egeberg, P. Blom, K.G. Knudsen, Top. Catal. 52 (2009) 229.
[17] V.N. Bui, D. Laurenti, P. Afanasiev, C. Geantet, Appl. Catal. B, Environ. 101 (2011) 239.
[18] V.N. Bui, D. Laurenti, P. Delichère, C. Geantet, Appl. Catal. B, Environ. 101 (2011) 246.
[19] Y. Romero, F. Richard, S. Brunet, Appl. Catal. B, Environ. 98 (2010) 213.
[20] P. Raybaud, Appl. Catal. A: Gen. 322 (2007) 76.
[21] J.-F. Paul, S. Cristol, E. Payen, Catal. Today 130 (2008) 139.

[22] N-Y. Topsøe, A. Tuxen, B. Hinnemann, J.V. Lauritsen, K.G. Knudsen, F. Besenbacher, H. Topsøe, J. Catal. 279 (2011) 337.
[23] C. Dupont, R. Lemeur, A. Daudin, P. Raybaud, J. Catal. 279 (2011) 276.
[24] G. Berhault, A. Mehta, A.C. Pavel, J. Yang, L. Redon, M.J. Yacaman, L.C. Araiza, A.D. Moller, R.R. Chianelli, J. Catal. 198 (2001) 9.
[25] Y. Iwata, K. Sato, T. Yoneda, Y. Miki, Y. Sugimoto, A. Nishijma, H. Shimada, Catal. Today 45 (1998) 353.
[26] S. Fuentes, G. Diaz, F. Fedraza, H. Rojas, N. Rosas, J. Catal. 113 (1988) 535.
[27] I. Bezverkhyy, M. Danot, P. Afanasiev, Inorg. Chem. 42 (2003) 1764.
[28] C.D. Wagner, W.M. Riggs, L.E. Davis, J.F. Moulder, Handbook of X-ray photoelectron spectroscopy, (G.E. Muilenberg, eds), Perkin-Elmer Corporation (Physical Electronics) (1979).
[29] A.D. Gandubert, C. Legens, D. Guillaume, S. Rebours, E. Payen, Oil Gas Sci. Technol. – Rev. IFP 62 (1) (2007) 79.
[30] A.D. Gandubert, E. Krebs, C. Legens, D. Costa, D. Guillaume, P. Raybaud, Catal. Today 130 (2008) 149.
[31] K. Marchand, C. Legens, D. Guillaume, P. Raybaud, OGST – Rev. IFP 64 (6) (2009) 719.
[32] G. Kresse, J. Hafner, Phys. Rev. B 47 (1993) 558.
[33] G. Kresse, J. Furthmüller, Phys. Rev. B 54 (1996) 11169.
[34] J.P. Perdew, Y. Wang, Phys. Rev. B 45 (1992) 13244.
[35] J.P. Perdew, J.A. Chevary, S.H. Vosko, K.A. Jackson, M.R. Pederson, D.J. Singh, C. Fiolhais, Phys. Rev. B 46 (1992) 6671.
[36] G. Kresse, D. Joubert, Phys. Rev. B 59 (1999) 1758.
[37] E. Krebs, B. Silvi, P. Raybaud, Catal. Today 130 (2008) 160.
[38] Y. Aray, D. Vega, J. Rodriguez, A.B. Vidal, M.E. Grillo, S. Coll, J. Phys. Chem. B 113 (2009) 3058.
[39] A. Daudin, S. Brunet, G. Pérot, P. Raybaud, C. Bouchy, J. Catal. 248 (2007) 111.
[40] A. Daudin, T. Chapus, Prepr. Pap. – Am. Chem. Soc. Div. Petr. Chem. 54 (2) (2009) 122.
[41] T.A. Pecoraro, R.R. Chianelli, J. Catal. 67 (1981) 430.
[42] A. Daudin, A.F. Lamic, G. Pérot, S. Brunet, P. Raybaud, C. Bouchy, Catal. Today 130 (2008) 221.
[43] N. Guernalec, C. Geantet, T. Cseri, M. Vrinat, H. Toulhoat, P. Raybaud, Dalton Trans. 39 (2010) 8420.
[44] P. Raybaud, J. Hafner, G. Kresse, H. Toulhoat, J. Phys. Condens. Matter. 9 (1997) 11107.
[45] I. Kubickova, M. Snare, K. Eränen, P. Mäki-Arvela, D.Y. Murzin, Catal. Today 106 (2005) 197.
[46] P. Mäki-Arvela, I. Kubickova, M. Snare, K. Eränen, D.Y. Murzin, Energy Fuel 21 (2007) 30.
[47] T. Todorova, R. Prins, T. Weber, J. Catal. 246 (2007) 109.